Acta Cryst. (1984). A40, 184–195

International Union of Crystallography

Commission on Charge, Spin and Momentum Densities

Project on Comparison of Structural Parameters and Electron Density Maps of Oxalic Acid Dihydrate

Project Reporter: PHILIP COPPENS, *Department of Chemistry, State University of New York at Buffalo, Buffalo, NY* 14214, *USA*. Co-authors: J. DAM, S. HARKEMA AND D. FEIL, *Department of Chemical Physics, Twente University of Technology, PO Box* 217, *Enschede, The Netherlands*; R. FELD* AND M. S. LEHMANN, *Institut Max von Laue–Paul Langevin, Avenue des Martyrs, F*38042 *Grenoble, CEDEX* 156, *France*; R. GODDARD AND C. KRÜGER, *Max-Planck Institut für Kohlenforschung, D*-4330 *Mülheim/Ruhr, Federal Republic of Germany*; E. HELLNER, *Fachbereich Geowissenschaften, Universitat, Lahnberge, D*3350 *Marburg, Federal Republic of Germany*; H. JOHANSEN, *Department of Chemistry B, Chemical Physics, The Technical Institute of Denmark, DTH* 301, *DK*-2800 *Lyngby, Denmark*; F. K. LARSEN, *Kemisk Institute, Aarhus University, DK*-8000 *Aarhus C, Denmark*; T. F. KOETZLE AND R. K. MCMULLAN, *Department of Chemistry, Brookhaven National Laboratory, Upton, NY* 11973, *USA*; E. N. MASLEN, *University of Western Australia, Nedlands, WA* 6009, *Australia*; E. D. STEVENS† AND P. COPPENS, *Department of Chemistry, State University of New York at Buffalo, Buffalo, New York* 14214, *USA*

(*Received* 19 *April* 1983; *accepted* 5 *August* 1983)

Abstract

Results obtained from four X-ray and five neutron data sets collected under a project sponsored by the Commission on Charge, Spin and Momentum Densities are analyzed by comparison of thermal parameters, positional parameters and $X-N$ electron density maps. Three sets of theoretical calculations are also included in the comparison. Though several chemically significant features are reproduced in all the experimental density maps, differences in detail occur which caution against overinterpretation of the maps. Large differences between vibrational tensor elements U_{ij} are observed which can often not be corrected by the scaling of all temperature parameters in a set. Positional parameters are reproducible to precisions of 0·001 Å or better. The biggest discrepancies between theoretical and experimental deformation density maps occurs in the lone-pair regions where peaks are higher in the theoretical maps. However, this comparison may be affected by inadequacies in the thermal-motion formalism which must be invoked before experimental and theoretical maps can be compared in a quantitative way.

Introduction

At the IUCr Conference in Amsterdam in 1975 a project was proposed under which the charge density in one crystalline material would be studied by a number of laboratories in order to assess the reproducibility of experimental electron density maps. After some discussion oxalic acid dihydrate (Fig. 1) was selected as the subject of the study. It is a relatively hard stable substance, of which crystals can be easily grown. An earlier study of deuterooxalic acid by X-rays and neutrons (Delaplane & Ibers, 1969; Sabine, Cox & Craven, 1969; Coppens & Sabine 1969; Coppens, Sabine, Delaplane & Ibers, 1969) indicated extinction to be severe, a possible argument against its choice as a calibration substance. However, as described below, extinction was much less severe in the samples used in this project.

Rather than distribute a crystal specimen and prescribe data collection and refinement procedures to be followed, crystals were grown by the participants and procedures commonly applied in each of the

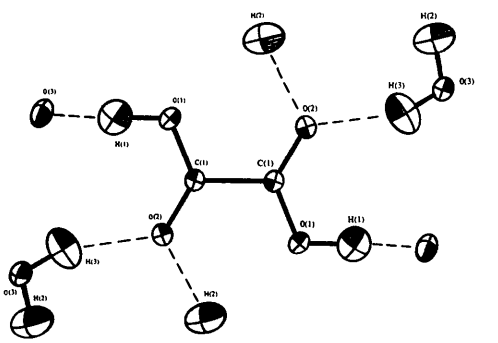

Fig. 1. *ORTEP* (Johnson, 1965) drawing of oxalic acid dihydrate and labeling of the atoms.

* Present address: Battelle-Institut e.V., Am Römerhof 35, D-6000 Frankfurt am Main 90, Federal Republic of Germany.

† Present address: Department of Chemistry, University of New Orleans, New Orleans, LA 70122, USA.

0108-7673/84/030184-12$01.50

Table 1. *Information on data collection*

	λ	Mono-chromator	Beam homogeneity	Crystal size (mm)	Orientation*	Temperature (K)†	Temperature calibration	Cooling method	Background correction	Scan width ω (°)	sin θ/λ (Å^{-1})
*X*1	Mo *Kα*	Graphite	No deviation	0·27×0·20×0·25	[107]	100±3	NI‡	N_2 stream	Stationery background measurement	NI‡	1·1
*X*2	Mo *Kα*	Graphite	Corrected¶¶	0·46×0·30×0·37	[010] within 20°	100±2	KDP§ 122 K	N_2 stream	Peak 1·25 + 0·75 tan θ	213 + 0·5 tan θ	1·3
*X*3	Mo *Kα*	Nb filter	No deviation	0·41×0·27×0·52	NI‡	100±1	KDP§ 122 K	N_2 stream	LL‡‡	θ(*Kα*$_1$ − 0·375) to θ(*Kα*$_2$ + 0·375)	1·20
*X*4	Mo *Kα*	Graphite	Unknown	0·27×0·32×0·60	NI‡	103±0·5	NI‡	N_2 stream	§§	0·7 + 0·35 tan θ	1·36
*N*1	0·862	Cu(220)	No deviation	2·7×2·7×2·7	[001]	100±1	KDP§ 122·4 K	He refrigerator**	LL‡‡ with straight-line background	NI‡	0·96
*N*2	0·525	Cu(200)	No deviation	3·1×3·1×3·1	[001]	100±1	KDP§ 122·4 K	He refrigerator**	LL‡‡ with straight-line background	NI‡	1·01
*N*3	0·862	Cu(220)	No deviation	2·7×2·7×2·7	[001]	75±1	KDP§ 122·4 K	He refrigerator**	LL‡‡ with straight-line background	NI‡	0·96
*N*4	0·8213 (2)	Ge(331)	NI‡	2·8×2·8×2·8	[20$\bar{1}$]	100±05	FeF_2¶ 78·38 K	He refrigerator††	Background from first and last tenth of each scan	1·05 + 1·23 tan θ above 25°, 1·5° below	0·997
*N*5	1·070	Be(002)	Better than 3%	3·0×3·0×3·0	[50$\bar{3}$]	115±1	NI‡‡	N_2 stream	LL‡‡	1·80 + 1·38 tan θ	0·78

* Direction of φ axis.
† Second number indicates temperature stability, not estimate of error in temperature estimate.
‡ NI: no information available.
§ Tetragonal-to-orthorhombic transition in KH_2PO_4 (Frazer & Pepinsky, 1953).
¶ Magnetic transition in FeF_2 at $T = 78{\cdot}38\,(1)$ K (Hutchings, Schulhof & Guggenheim, 1972).
** Allibon, Filhol, Lehmann, Mason & Simms (1981).
†† Air Products and Chemicals Displex Model CS-202.
‡‡ Lehmann & Larsen (1974).
§§ Time spent measuring background was half that taken to measure the peak.
¶¶ Harkema, Dam, Van Hummel & Reuvers (1980).

Table 2. *Information on least-squares refinements*

	NO* before averaging	NO* after averaging	F/F^2†	$\sigma^2(F^2)$†	Weak reflections	Extinction	Scattering factors	Anomalous scattering	R‡	R_w‡	S‡	High-order cut-off (Å^{-1})	High-order refinement NO*	R	R_w	S
*X*1			F^2	$\sigma^2_{count}+0{\cdot}002\,F^4$	NI§	Anisotropic Type I Lorentzian¶	IT**	NI	4·2 4·7	4·0 8·1	2·7	0·85	818	6·9 4·8	8·4 10·5	1·83
*X*2	46994	3304	F	$\sigma^2_{count}+0{\cdot}0009\,F^4$††	$I<3\sigma$ eliminated	Isotropic	IT+SDS‡‡	CL§§	3·1	3·5	3·49	1·0	1479	4·0	2·7	1·28
*X*3	10692	2315	F	$\sigma^2_{count}+0{\cdot}0004\,F^4$¶¶	$F<2\sigma$ eliminated	Isotropic type I Lorentzian	IT+SDS	CL§§	2·64	3·79	2·53	1·0	463	5·52	2·04	1·38
*X*4	5799	3091	F	$\sigma^2_{count}+0{\cdot}0004\,F^4$	$I<2\sigma$ eliminated	No improvement	CW*** SDS‡‡	Not included	4·3	5·4	2·7	1·0	1400	5·2	4·7	1·25
*N*1	3700	1781	F^2	$\sigma^2_{count}+0{\cdot}002\,F^4$	$F^2<3\sigma$ eliminated	No improvement	†††	—	2·94 3·64	3·70 6·46	1·127					
*N*2	3403	1824	F^2	$\sigma^2_{count}+0{\cdot}002\,F^4$	$F^2<3\sigma$ eliminated	Anisotropic type I Lorentzian	†††	—	6·42 5·24	5·86 9·60	1·281					
*N*3	3700	1781	F^2	$\sigma^2_{count}+0{\cdot}002\,F^4$	$F^2<3\sigma$ eliminated	Anisotropic type I Lorentzian	†††	—	2·88 4·04	3·60 3·60	NI					
*N*4	3797	1912	F^2	$\sigma^2_{count}+0{\cdot}0001\,F^4$		Anisotropic type I Lorentzian‡‡‡	†††	—	4·5	4·6	1·15					
*N*5	850	554	F^2	$\sigma^2_{count}+0{\cdot}0004\,F^4$	$F^2<2\sigma$ eliminated	Anisotropic type I Lorentzian	§§§	—	2·9 5·0	3·4 6·8	2·42					

* NO: number of observations.

† Function minimized $\sum w(Y_{obs}-k^nY_{calc})$, where $Y=F^n$, $w=1/\sigma^2(Y)$ and $n=1$ or 2.

‡ When 2 entries are given, first is $R(F)$ second $R(F^2)$, a single entry corresponds to power of F listed in column 3. S = goodness of fit is defined as $(\sum w\Delta^2/n-m)^{1/2}$, where n = number of observations, m = number of variables.

§ NI: no information available.

¶ Becker & Coppens (1974, 1975); Thornley & Nelmes (1974).

** *International Tables for X-ray Crystallography* (1974).

†† For part of the reflections $\sigma^2=\sigma^2_{count}+0{\cdot}0036\,F^4$.

‡‡ Stewart, Davidson & Simpson (1965).

§§ Cromer & Libermann (1970).

¶¶ The mean-square deviation over symmetry equivalents was taken as σ^2 if its value was larger than σ^2.

*** Cromer & Waber (1965).

††† $b_H=-3{\cdot}7409$ fm; $b_C=6{\cdot}6486$ fm; $b_O=5{\cdot}8030$ fm (Koester, 1977).

‡‡‡ 55 strongly extinction affected reflections were omitted from the best refinement.

§§§ $b_H=-3{\cdot}74$ fm; $b_C=6{\cdot}65$ fm; $b_O=5{\cdot}80$ fm (Bacon, 1975).

laboratories were used. The philosophy behind this choice is that the results may truly reflect the spread between results from different laboratories rather than be biased by peculiarities of one or two crystals and selection of a single interpretive method.

Four X-ray data sets were collected, while five neutron data sets were measured in three different laboratories. Two other X-ray data sets collected while the project was being undertaken were not judged of adequate quality by the experimenters and were therefore not submitted to the project.

Three sets of theoretical calculations were made by two participants in different institutions. Two of these use extended basis sets, while in the third a limited basis set was employed.

In this report details of data collection and refinement and of the theoretical calculations are summarized first. The remainder of the report concerns the comparison of parameters and electron density maps obtained by various research groups. Since different crystals were used and details of the refinement procedures varied, the comparison provides the first estimate of the reliability of experimental results of this kind including the effects of systematic errors. The comparison is somewhat restricted by the limited number of data sets contributed to the project. Nevertheless, we believe that it does provide an indication of the reproducibility of experimental charge densities.

Experimental details

Details on data collection are summarized in Table 1. All X-ray data-collection temperatures were reported to be close to 100 K, while one of the neutron experiments (*N*3) was performed at 75 K on a crystal that also was studied at 100 K. An additional experiment (*N*5) was done at 115 K. Mo $K\alpha$ radiation was used in all the X-ray experiments; neutron experiments are less standardized and four different wavelengths ranging from 1·070 to 0·525 Å were used.

All refinements assigned least-squares weights based on $\sigma^2(F^2)=\sigma^2_{\text{counting}}+c^2F^4$ with c^2 varying between 0·0020 and 0·0001 indicating estimates of the proportional error in the intensity measurement, ranging from 4·5 to 1%. Information about the least-squares refinements is given in Table 2. Though extinction was treated in the least-squares refinement of all the X-ray data sets, it was much less severe than in the samples used in the room-temperature studies reported in 1969, the y values ($y=F^2_{\text{obs}}/F^2_{\text{corr}}$) being typically larger than 0·85 for the most severely affected reflections. In the neutron experiments extinction was more severe and best described in all refinements by a type I crystal with a Lorentzian distribution of the mosaic spread.

Though X-ray R factors vary, the goodness of fit S is similar for the four full-data refinements. The high-order refinement of *X*1 with a lower ($\sin\theta/\lambda$) limit of 0·85 Å^{-1} shows a larger value of S than the other refinements in which cut-off values of 1·0 Å^{-1} were used. This may indicate the need for the higher cut-off if model bias is to be eliminated from the refinement.

Table 3. *Theoretical calculations*

	Basis set* C, N, O	Basis set* H	Energy (a.u.)
*T*1	11, 6, 1/5, 3, 1	6, 1/3, 1	−376·4864
*T*2	11, 5, 1/4, 3, 1†	6, 1/4, 1	−376·4458
*T*3	8, 4, 0/3, 2, 0‡	4, 0/2, 0	−375,7790

* *A*, *B*, *C*/*D*, *E*, *F* represents *A* *s*-type, *B* *p*-type, and *C* *d*-type primitives contracted to *D*, *E*, *F* *s*, *p*, *d*-type functions.
† Pople & Binkley (1979); 2*s* and 2*p* functions share exponent.
‡ 4-31G basis; Ditchfield, Hehre & Pople (1971).

Theoretical studies

Theoretical molecular-orbital wave functions were calculated for the oxalic acid molecule using *ab initio* self-consistent field methods (Roothaan, 1951) and basis sets of Gaussian orbitals. The size of the basis sets and the molecular electronic energies are summarized in Table 3. Two of the basis sets (*T*1 and *T*2) contain polarization functions and are commonly described as extended basis sets (EBS); the third is a more limited set without *d* functions on the C and O atoms or *p* functions on the hydrogen atoms.

Calculations summarized here were performed for the isolated molecule with the geometry determined by the earlier neutron diffraction experiment (Coppens & Sabine, 1969), which is in close agreement with the present results except for the O(1)–H(1) bond length which is 1·026 (7) Å at room temperature, but 1·07 (1) Å at 100 K.

The lowest energy is obtained with the largest of the two EBS sets, while the limited set used in *T*3 is clearly less favorable than the bases used in either *T*1 or *T*2.

Comparison of diagonal elements of thermal motion tensors

(*a*) *Comparison of X-ray sets*

A comparison of X-ray thermal parameters is made in Table 4. It is clear from the table that discrepancies are frequently much larger than what might be expected on the basis of the least-squares standard deviations. A statistical analysis of the $\Delta/\sigma(\Delta)$ ratios $[\Delta_{IJ}=(U_{ij})_{\text{set }I}-(U_{ii})_{\text{set }J}]$, not reported in detail here, shows the discrepancies to be highly significant.

The U_{33} ratios of X_2/X_1, X_1/X_4 and X_1/X_3 are particularly anomalous, relative to the values of the U_{11} and U_{22} ratios, indicating a systematic anisotropic error in the *X*1 experiment. Similarly, the U_{22} ratios

Table 4. *Temperature parameter ratios between X-ray sets*

U	Average*	C	O(1)	O(2)	O(3)
	*X*2(100 K)/*X*1(100 K)				
11	1·013 (0·010)	1·000 (0·018)	1·012 (0·013)	1·025 (0·015)	1·018 (0·015)
22	1·016 (0·012)	0·999 (0·017)	1·021 (0·011)	1·024 (0·011)	1·021 (0·012)
33	0·756 (0·010)	0·755 (0·015)	0·744 (0·013)	0·769 (0·012)	0·758 (0·012)
	*X*2(100 K)/*X*3(100 K)				
11	0·932 (0·009)	0·926 (0·011)	0·941 (0·008)	0·923 (0·009)	0·939 (0·008)
22	0·912 (0·016)	0·888 (0·010)	0·922 (0·006)	0·919 (0·007)	0·919 (0·007)
33	0·947 (0·010)	0·950 (0·013)	0·948 (0·010)	0·932 (0·009)	0·957 (0·010)
	*X*2(100 K)/*X*4(103 K)				
11	0·757 (0·004)	0·753 (0·008)	0·757 (0·006)	0·763 (0·007)	0·754 (0·007)
22	0·690 (0·015)	0·712 (0·007)	0·678 (0·006)	0·684 (0·006)	0·686 (0·006)
33	0·762 (0·003)	0·759 (0·010)	0·762 (0·010)	0·766 (0·008)	0·761 (0·008)
	*X*1 (100 K)/*X*4 (103 K)				
11	0·747 (0·005)	0·753 (0·014)	0·749 (0·010)	0·745 (0·011)	0·741 (0·011)
22	0·679 (0·023)	0·713 (0·012)	0·664 (0·008)	0·668 (0·009)	0·672 (0·009)
33	1·008 (0·012)	1·006 (0·020)	1·024 (0·019)	0·997 (0·016)	1·004 (0·016)
	*X*1 (100 K)/*X*3 (100 K)				
11	0·920 (0·013)	0·926 (0·018)	0·930 (0·012)	0·901 (0·013)	0·923 (0·014)
22	0·897 (0·006)	0·889 (0·016)	0·903 (0·011)	0·898 (0·010)	0·900 (0·011)
33	1·252 (0·027)	1·259 (0·025)	1·275 (0·022)	1·212 (0·018)	1·262 (0·020)
	*X*4 (103 K)/*X*3 (100 K)				
11	1·232 (0·016)	1·230 (0·014)	1·243 (0·011)	1·210 (0·012)	1·246 (0·011)
22	1·323 (0·051)	1·247 (0·013)	1·360 (0·012)	1·345 (0·013)	1·339 (0·013)
33	1·242 (0·018)	1·251 (0·017)	1·245 (0·017)	1·216 (0·013)	1·257 (0·014)

* Standard deviation in average calculated from spread of sample; standard deviation in individual ratios from least-squares results.

Table 5. U_{ii} *ratios*: $\langle U_{ii}/U_{ii}\rangle$

Numerator = set listed in first row, denominator = set listed in first column.

	*X*1 (100 K)	*X*2 (100 K)	*X*3 (100 K)	*X*4 (103 K)	*N*1 (100 K)	*N*2 (100 K)	*N*4 (100 K)	*N*5 (115 K)
*X*1	—	0·93	0·98	1·23	0·80	0·83	0·88	0·83
*X*2	1·08	—	1·07	1·36	0·87	0·91	0·97	0·90
*X*3	1·02	0·93	—	1·27	0·81	0·85	0·91	0·83
*X*4	0·81	0·74	0·79	—	0·64	0·67	0·72	0·66
*N*1	1·26	1·14	1·33	1·56	—	1·03	1·08	1·02
*N*2	1·20	1·10	1·18	1·49	0·97	—	1·06	1·00
*N*4	1·14	1·03	1·10	1·40	0·92	0·95	—	0·94
*N*5	1·21	1·11	1·20	1·52	0·98	1·00	1·06	—

for X_4/X_3 and X_4/X_2 are too high, suggesting a smaller but still significant effect in $X4$. The best consistency is found for X_2/X_3 for which an average ratio of 0·93 is obtained with only small deviations from the average value. The uniformity of the ratio suggests that the discrepancy may be due to different data-collection temperatures, or perhaps differences between TDS contributions. Averages of all the U_{ii} ratios summarized in Table 5 show the $X4$ experiment to deviate from the main body of experiments. Possible causes of this discrepancy are discussed in the next section.

On the other hand, the spread among individual atoms within one U_{ii} ratio is small; for each comparison of all U_{ii} ratios for one value of i are similar, while differences between rows are pronounced. This implies that in a rigid-body analysis of vibrational parameters much of the discrepancy will be absorbed in the translational rather than the librational mean-square displacements.

(*b*) *Comparison of neutron sets* (*Table* 6)

The neutron temperature parameters appear better reproducible than the X-ray results, except for experiment $N5$ which, given the 115 K data collection temperature, has anomalously low U_{11} and U_{22} values. The $N3/N1$ ratio is in good agreement with what may be expected on the basis of the temperature difference.

(*c*) *X-ray–neutron comparison* (*Table* 7)

Since $X3$ and $X2$ appear to be the most consistent X-ray data sets their temperature parameters are compared with the corresponding neutron parameters of $N1$ and $N4$ in Table 7. The best agreement is obtained between $X2$ and $N4$, though even in this case individual deviations often exceed statistical criteria. $X3$ appears to have been collected at a somewhat higher temperature than both $N1$ and $N4$.

Table 6. *Selected temperature parameter ratios between neutron sets*

U	Average	C	O(1)	O(2)	O(3)	H(1)	H(2)	H(3)
	*N*2 (100 K)/ *N*1 (100 K)							
11	0·989 (0·021)	0·968 (0·019)	0·986 (0·018)	0·998 (0·018)	0·999 (0·019)	0·995 (0·022)	0·956 (0·022)	1·020 (0·022)
22	1·046 (0·031)	1·100 (0·020)	1·041 (0·016)	1·044 (0·016)	1·062 (0·016)	1·053 (0·023)	1·014 (0·022)	1·008 (0·022)
33	1·052 (0·044)	1·066 (0·025)	1·116 (0·030)	1·074 (0·025)	1·076 (0·027)	0·989 (0·025)	1·005 (0·025)	1·035 (0·023)
	*N*4 (100 K)/ *N*1 (100 K)							
11	1·117 (0·052)	1·152 (0·015)	1·134 (0·014)	1·153 (0·014)	1·185 (0·015)	1·066 (0·015)	1·074 (0·016)	1·052 (0·015)
22	1·092 (0·054)	1·165 (0·014)	1·120 (0·011)	1·120 (0·011)	1·123 (0·011)	1·063 (0·014)	1·037 (0·014)	1·018 (0·013)
33	1·057 (0·031)	1·069 (0·016)	1·086 (0·019)	1·087 (0·016)	1·081 (0·016)	1·018 (0·015)	1·024 (0·015)	1·030 (0·013)
	*N*5 (115 K)/ *N*1 (100 K)							
11	0·975 (0·085)	0·946 (0·059)	1·117 (0·054)	0·930 (0·051)	0·941 (0·058)	1·065 (0·055)	0·950 (0·058)	0·874 (0·050)
22	0·973 (0·032)	0·912 (0·042)	0·957 (0·033)	0·976 (0·035)	0·981 (0·037)	0·981 (0·044)	0·993 (0·041)	1·014 (0·040)
33	1·117 (0·086)	1·082 (0·057)	1·195 (0·073)	1·211 (0·059)	1·215 (0·062)	1·033 (0·062)	1·050 (0·053)	1·034 (0·045)
	*N*5 (115 K)/ *N*4 (100 K)							
11	0·875 (0·085)	0·821 (0·050)	0·985 (0·048)	0·807 (0·044)	0·794 (0·049)	1·000 (0·052)	0·884 (0·054)	0·831 (0·048)
22	0·894 (0·071)	0·782 (0·035)	0·855 (0·029)	0·871 (0·031)	0·873 (0·033)	0·923 (0·041)	0·958 (0·040)	0·997 (0·039)
33	1·056 (0·053)	1·012 (0·053)	1·100 (0·067)	1·114 (0·054)	1·124 (0·056)	1·015 (0·061)	1·025 (0·051)	1·005 (0·043)
	*N*3 (75 K)/ *N*1 (100 K)							
11	0·810 (0·079)	0·759 (0·032)	0·729 (0·030)	0·730 (0·031)	0·782 (0·030)	0·865 (0·028)	0·889 (0·029)	0·919 (0·027)
22	0·875 (0·056)	0·845 (0·021)	0·825 (0·014)	0·826 (0·014)	0·846 (0·014)	0·883 (0·018)	0·967 (0·018)	0·933 (0·009)
33	0·850 (0·093)	0·835 (0·045)	0·836 (0·054)	0·768 (0·038)	0·732 (0·039)	1·017 (0·031)	0·854 (0·030)	0·906 (0·023)

Table 7. *Selected temperature parameter ratios between X-ray and neutron sets*

U	Average	C	O(1)	O(2)	O(3)
(*a*) All data					
	*X*3 (100 K)/ *N*1 (100 K)				
11	1·202 (0·015)	1·223 (0·017)	1·201 (0·014)	1·194 (0·014)	1·191 (0·014)
22	1·276 (0·048)	1·336 (0·018)	1·266 (0·012)	1·220 (0·011)	1·283 (0·012)
33	1·212 (0·051)	1·239 (0·019)	1·162 (0·019)	1·270 (0·018)	1·178 (0·017)
	*X*3 (100 K)/ *N*4 (100 K)				
11	1·040 (0·026)	1·062 (0·012)	1·058 (0·011)	1·036 (0·011)	1·005 (0·010)
22	1·127 (0·026)	1·147 (0·012)	1·130 (0·009)	1·089 (0·009)	1·142 (0·010)
33	1·121 (0·049)	1·158 (0·015)	1·070 (0·014)	1·168 (0·012)	1·089 (0·012)
	*X*2 (100 K)/ *N*1 (100 K)				
11	1·121 (0·014)	1·133 (0·015)	1·130 (0·012)	1·102 (0·012)	1·118 (0·013)
22	1·163 (0·029)	1·187 (0·014)	1·167 (0·010)	1·122 (0·010)	1·178 (0·010)
33	1·147 (0·039)	1·177 (0·018)	1·102 (0·017)	1·183 (0·016)	1·127 (0·016)
	*X*2 (100 K)/ *N*4 (100 K)				
11	0·970 (0·024)	0·984 (0·010)	0·996 (0·009)	0·956 (0·010)	0·944 (0·010)
22	1·028 (0·022)	1·018 (0·010)	1·042 (0·008)	1·001 (0·008)	1·049 (0·008)
33	1·061 (0·040)	1·100 (0·014)	1·014 (0·012)	1·088 (0·011)	1·042 (0·011)
(*b*) High-order data					
	*X*1(HO) (100 K)/ *N*1 (100 K)				
11	1·096 (0·026)	1·129 (0·025)	1·098 (0·019)	1·068 (0·019)	1·088 (0·020)
22	1·158 (0·053)	1·234 (0·026)	1·151 (0·017)	1·113 (0·017)	1·133 (0·017)
33	1·484 (0·039)	1·483 (0·038)	1·441 (0·034)	1·536 (0·032)	1·475 (0·031)
	*X*2(HO) (100 K)/ *N*4 (100 K)				
11	0·945 (0·011)	0·941 (0·010)	0·961 (0·010)	0·938 (0·010)	0·940 (0·010)
22	1·016 (0·006)	1·018 (0·012)	1·022 (0·009)	1·008 (0·009)	1·016 (0·009)
33	1·023 (0·012)	1·038 (0·013)	1·014 (0·013)	1·025 (0·011)	1·013 (0·011)
	*X*3(HO) (100 K)/ *N*4 (100 K)				
11	1·019 (0·009)	1·024 (0·014)	1·022 (0·013)	1·025 (0·014)	1·006 (0·013)
22	1·103 (0·015)	1·124 (0·012)	1·086 (0·010)	1·102 (0·010)	1·102 (0·010)
33	1·042 (0·026)	1·072 (0·012)	1·018 (0·012)	1·054 (0·011)	1·021 (0·011)
	*X*4(HO) (103 K)/ *N*1 (100 K)				
11	1·459 (0·015)	1·474 (0·020)	1·448 (0·016)	1·444 (0·017)	1·471 (0·017)
22	1·664 (0·059)	1·752 (0·029)	1·643 (0·017)	1·624 (0·017)	1·636 (0·017)
33	1·482 (0·022)	1·511 (0·024)	1·485 (0·026)	1·466 (0·022)	1·464 (0·023)

(*d*) *Comparison of all-data and high-order (HO) X-ray refinements* (*Table* 8)

As valence electron scattering is concentrated in the low-order reflections, refinement of high-order data only is often used to reduce model bias resulting from the isolated-atom approximation. Since a small fraction of the valence electrons accumulate in the bonding region away from the atoms, X-ray temperature parameters obtained with the independent atom model tend to be somewhat larger than neutron or high-order-refinement values (Coppens, 1975).

Table 8. *Temperature parameter ratios between high-order (HO) and full-data X-ray refinements*

U	Average	C	O(1)	O(2)	O(3)
	*X*1(HO) (100 K)/*X*1 (100 K)				
11	0·991 (0·006)	0·997 (0·025)	0·983 (0·018)	0·993 (0·020)	0·990 (0·020)
22	1·011 (0·024)	1·039 (0·025)	1·007 (0·016)	1·015 (0·017)	0·981 (0·017)
33	0·979 (0·021)	0·952 (0·027)	0·973 (0·024)	0·998 (0·022)	0·992 (0·021)
	*X*2(HO) (100 K)/*X*2 (100 K)				
11	0·975 (0·018)	0·957 (0·010)	0·964 (0·008)	0·981 (0·008)	0·997 (0·009)
22	0·989 (0·018)	1·000 (0·012)	0·980 (0·008)	1·007 (0·008)	0·969 (0·007)
33	0·964 (0·028)	0·944 (0·012)	1·000 (0·011)	0·942 (0·009)	0·972 (0·009)
	*X*3(HO) (100 K)/*X*3 (100 K)				
11	0·980 (0·018)	0·964 (0·014)	0·966 (0·011)	0·990 (0·013)	1·001 (0·012)
22	0·979 (0·023)	0·980 (0·012)	0·961 (0·008)	1·012 (0·008)	0·965 (0·008)
33	0·930 (0·021)	0·926 (0·012)	0·952 (0·010)	0·903 (0·008)	0·937 (0·010)
	*X*4(HO) (103 K)/*X*4 (103 K)				
11	0·986 (0·013)	0·980 (0·011)	0·970 (0·008)	1·000 (0·009)	0·992 (0·009)
22	0·987 (0·046)	1·051 (0·015)	0·954 (0·010)	0·990 (0·011)	0·952 (0·010)
33	0·985 (0·032)	0·975 (0·014)	1·027 (0·015)	0·949 (0·011)	0·989 (0·012)

Table 9. *Comparison of cell dimensions*

	a (Å)	*b* (Å)	*c* (Å)	*β* (°)
Nitrogen temperature				
*X*1	6·103 (3)	3·498 (3)	11·978 (8)	105·87 (5)
*X*2	6·0986 (5)	3·4981 (3)	11·952 (1)	105·777 (8)
*X*3	6·0968 (7)	3·4975 (4)	11·9462 (15)	105·78 (1)
*X*4	6·1108 (9)	3·5109 (4)	11·9780 (8)	105·767 (8)
*N*1*	6·1016 (1)	3·4972 (1)	11·9549 (3)	105·759 (2)
*N*4	6·102 (3)	3·496 (2)	11·949 (5)	105·66 (4)
Room temperature†				
	6·119	3·607	12·057	106·19

* From measurement on a powder.
† Delaplane & Ibers (1969).

This trend is observed in experiments *X*2, *X*3 and *X*4, all of which show a 2–3% reduction in temperature parameters when high-order data are used. The lower data cut-off in experiment *X*1 was 0·85 Å^{-1} (Table 2). It appears that this cut-off is too low to reduce model bias adequately. The goodness of fit (Table 2) which is reduced to 1·38 and 1·25 in *X*3 and *X*4 is 1·83 for the *X*1 HO refinement, again indicating remaining model bias.

When *X*2 HO temperature parameters are compared with *N*4, values of 0·945, 1·016 and 1·023 are obtained for the U_{11}, U_{22} and U_{33} ratios, respectively (Table 7*b*). The average value of 0·995 is remarkably close to unity in this case.

(*e*) *Comparison of cell dimensions and discussion of temperature parameter discrepancies*

If a genuine difference between specimen temperatures exists, a parallel discrepancy may be expected in the cell dimensions, values of which are reported in Table 9. There is excellent agreement between *N*1, *N*4, *X*2 and *X*3. The *X*4 values are indeed larger, supporting the interpretation of the temperature-parameter differences as being due, at least partly, to a difference in data-collection temperature.

One group of participants has independently carried out a study of the temperature dependence of the cell dimensions of oxalic acid dihydrate (Dam, Harkema & Feil, 1982), and has drawn the conclusion that the *X*4 data-collection temperature was about 110 K rather than the value of 103 K reported here. Since mean-square vibrational amplitudes for a molecule such as oxalic acid are almost proportional to absolute temperature near 100 K, this temperature difference only partially explains the 20–40% increase in *X*4 temperature parameters. It is quite likely that a major origin of the discrepancy lies in the use of Dirac–Slater form factors in the *X*4 refinement (Table 2). These form factors are more compact than RHF (relativistic Hartree–Fock) values used in the other experiments and would thus naturally lead to larger temperature parameters.

Comparison of positional parameters

Since it was obvious on preliminary inspection that the positional parameters from the different experiments were in good agreement, a χ^2 test was performed to test the significance of any differences, For the X-ray results only non-hydrogen parameters were tested, giving a total of 12 contributions to χ^2. For the comparison between neutron results all seven atoms were included leading to a total of 21 parameters. The test compares values of $\chi^2 = \sum (\Delta/\sigma)^2$ with tabulated values at various significance levels (Hamilton, 1964). As $\chi^2(12)_{0.995}$ and $\chi^2(21)_{0.995}$ are 28·3 and 41·4, respectively, χ^2 values above these levels indicate discrepancies significant at the 0·995 confidence level.

Results listed in Table 10 show that: (*a*) the *X*4 experiment deviates from *X*2 and *X*3, a possible result of the temperature difference mentioned earlier which would affect coordinates as thermal expansion is different for inter- and intramolecular distances; (*b*) there are no significant differences between positional parameters from the four neutron experiments

even though $N5$ was reported to be performed at a higher temperature than the other experiments; (*c*) highly significant discrepancies between X-ray and neutron positional parameters exist (upper right rectangle of Table 10), which disappear (except for $X4$) when comparison is made with the high-order parameters, thus confirming the validity of the high-order refinement in eliminating positional parameter bias.

In Table 11 the averages over the absolute values of the discrepancies in Å are listed. The agreement between the X-ray sets are within a few ten-thousands of an ångstrom, again with the exception of $X4$, for which the discrepancies are about 0·001 Å. The agreement between the X-ray sets $X2$ and $X3$ and the neutron sets $N1$, $N2$ and $N4$ averages to 0·0004–0·0006 Å when high-order X-ray results are used, an impressive demonstration of the reproducibility that accurate diffraction studies can provide. Of course, the interpretation of such precise values requires an understanding of the averaging of the positional parameters over the vibrational modes of the crystal.

Electron density maps

Deformation density maps defined as

$$\Delta\rho(\mathbf{r}) = \rho_{\text{obs}}(\mathbf{r}) - \rho(\mathbf{r})_{\text{calc, spherical atoms}}$$

are calculated with the expression

$$\Delta\rho(\mathbf{r}) = \frac{2}{V}\sum (F_{\text{obs}}/k - F_{\text{calc}}) \cos(2\pi\mathbf{H}\,.\,\mathbf{r}).$$

Table 10. *χ^2 values for positional parameter differences*

$\chi^2 = \sum(\Delta/\sigma)^2$.

	$X1$	$X2$	$X3$	$X4$	$N1$	$N2$	$N4$	$N5$
		All data				All data*		
$X1$	—	22·6	24·2	54·7	96·6	62·8	92·2	25·1
$X2$	—	—	15·2	87·6	101·7	39·0	97·2	18·9
$X3$	—	—	—	48·8	125·9	44·5	111·7	18·6
$X4$	—	—	—	—	124·6	43·2	108·3	20·2
		High order*				All data†		
$N1$	29·1	21·1	19·3	48·8	—	26·5	20·9	26·5
$N2$	27·9	4·3	10·8	17·7	—	—	24·3	28·7
$N4$	34·7	22·6	17·9	42·8	—	—	—	27·9
$N5$	16·7	13·7	11·5	18·0	—	—	—	—

* Sum of 12 values $\chi^2(12)_{0.995} = 28.3$.
† Sum of 21 values $\chi^2(21)_{0.995} = 41.4$.

Here k is the scale factor and F_{calc} is obtained with free-atom form factors and positional and structural parameters from the neutron or high-order X-ray refinements, described as $X-N$ and $X-X$ maps, respectively.

The maps compared in this report are based on combining the $X4$ and $X1$ data sets with $N1$ neutron results and $X3$ with the $X4$ neutron parameters; for $X2$ high-order parameters were used for C and O, while hydrogen parameters were taken from $N4$. In the case of $X3$, neutron temperature parameters were scaled by the average ratio of $U_{ii,X3(\text{HO})}/U_{ii,N4}$ for the heavy atoms giving a correction factor of 1·06; no such scaling was applied in the other combinations of X-ray and neutron data. The corresponding ratios for $X1(\text{HO})/N1$, $X2(\text{HO})/N4$ and $X4(\text{HO})/N1$ are 1·25, 0·99 and 1·54, respectively.

The maps obtained experimentally are thermally smeared over the vibrations of the crystal, while theoretical maps are for the static molecule. A quantitative comparison between theory and experiment requires convolution of the static theoretical density with the thermal probability distribution function, or deconvolution of the experimental results by fitting of static density functions to the experimental density using a formalism in which thermal motion is explicitly accounted for (*e.g.* Coppens, 1982). Of the theoretical maps based on $T2$ and $T3$ thermally smeared versions are available, while static multipole model maps have been calculated based on $X3$. Nevertheless, it must be kept in mind that quantitative comparison between theory and experiment is subject to inadequacies in the thermal-motion formalism.

In the following we will first compare bond and lone-pair peak heights and subsequently consider the more detailed features of the electron distribution in the plane of the oxalic acid molecule.

(*a*) *Peak heights* (*Table* 12)

There is a general tendency for peak heights in the $X1$ and $X4$ maps to be larger than for $X2$ and $X3$. This tendency, which is especially pronounced in the oxygen lone-pair regions of $X1$, is probably related to the large values of the $U_{ii,X}/U_{ii,N}$ ratios for $X1$

Table 11. *Average values of positional parameter discrepancies* (Å)

	$X1$	$X2$	$X3$	$X4$	$N1$	$N2$	$N4$	$N5$
		All data				All data		
$X1$	—	0·0006	0·0006	0·0012	0·0011	0·0014	0·0012	0·0016
$X2$	—	—	0·0003	0·0011	0·0008	0·0009	0·0007	0·0013
$X3$	—	—	—	0·0010	0·0010	0·0009	0·0009	0·0013
$X4$	—	—	—	—	0·0015	0·0013	0·0014	0·0015
		High order				All data		
$N1$	0·0011	0·0004	0·0005	0·0010	—	0·0010	0·0006	0·0019
$N2$	0·0013	0·0004	0·0006	0·0008	—	—	0·0010	0·0021
$N4$	0·0011	0·0005	0·0005	0·0010	—	—	—	0·0022
$N5$	0·0015	0·0012	0·0011	0·0016	—	—	—	—

Table 12. *Bond and lone pair peak heights* (e Å^{-3})

	Dynamic, experiment				Dynamic, theory	
	*X*1–*N*1	*X*2–*N*4	*X*3–*N*4	*X*4–*N*1	*T*2	*T*3
C(1)–C(1)	0·52 (0·77)*	0·56	0·69	0·67	0·58	0·38
C(1)–O(1)	0·75	0·37	0·49	0·52	0·43	0·20
C(1)–O(2)	0·52	0·46	0·55	0·67	0·62	0·46
O(1)–H(1)	0·85	0·32	0·33	0·51	0·40	0·23
O(1)l.p.	1·15	0·32	0·49	0·57	0·60	0·73
O(2)l.p.	0·85	0·27	0·41	0·46	0·53	0·61
O(2)l.p.	0·75	0·22	0·31	0·47	0·53	0·64

	Static, experiment		Static, theory		
	*X*3†	*X*3‡	*T*1	*T*2	*T*3
C(1)–C(1)	0·65	0·64	0·77	0·67	0·40
C(1)–O(1)	0·60	0·58	0·55	0·54	0·25
C(1)–O(2)	0·85	0·79	0·72	0·70	0·54
O(1)–H(1)	0·55	0·62	0·55	0·56	0·34
O(1)l.p.	0·68	0·93	1·09	1·10	1·18
O(2)l.p.	0·44	0·61	1·29	1·22	1·49
O(2)l.p.	0·42	0·54	1·33	1·32	1·39

* First value: at centre of bond; value in parentheses: maximum.
† Static map calculated from multipole model functions of X-ray refinement.
‡ Static map calculated from joint refinement of structural and multipole model parameters using *X*3 and *N*4 data.

and *X*4, though we note that the peak heights are largest for *X*1, while the ratio is largest for *X*4/*N*1. The use of different form factors in the *X*4 calculation is an additional factor influencing peak heights.

The agreement between *X*2 and *X*3 is within about 0·15 e Å^{-3} and probably as good as may be expected from present-day charge-density studies of the type reported here.

Examination of the primary theoretical results, the static values, indicates quite reasonable agreement, within about 0·1 e Å^{-3} and often better, between the two extended-basis-set calculations *T*1 and *T*2.

The limited-basis-set calculation *T*3 clearly does not produce a satisfactory density and underestimates bond peak values while overestimating the heights of peaks in the lone-pair regions.

When the *T*1 and *T*2 results are compared with *X*3 at the static level and with *X*2 and *X*3 in the dynamic case, agreement is again within 0·1 e Å^{-3} for the bond peaks, while the lone-pair peaks are either too low in the experiment or too high even in the EBS calculations *T*1 and *T*2. This may be due to either remaining basis-set truncation errors or other imperfections in the theoretical treatment or to inadequacies in the thermal-motion treatment required for the comparison between theory and experiment.

(*b*) *Direct comparison of electron density maps in the oxalic acid plane*

For practical reasons comparison of density maps will be mainly limited to the density in the plane of the oxalic acid molecule. The pertinent maps are shown in Fig. 2. Though the main features of the maps are reproduced in all experiments, there is considerable difference in detail. Not unexpectedly this is evident in the regions immediately surrounding the nuclei where the experimental errors in the deformation density are largest, but also in some of the other features. The largest deviations are observed in the *X*1 map, which shows a double maximum in the C–C bond and also differs in the location of the lone-pair maxima near the oxygen atoms. But this map also has much larger fluctuations in the background region away from the molecule and is therefore probably less reliable, in agreement with the higher *R* factors and somewhat inconsistent temperature-factor ratios obtained in this experiment.

The *X*4 and *X*2 maps share the general shape of the maxima which have a rounded rather than the more squarely shaped form observed in the *X*3 map, especially in the carbon–carbon bond. On the other hand, *X*4 and *X*2 differ markedly in the position of the zero contour around the molecule and near the atom centers. The latter difference may well be related to the use of a different spherical-atom form factor in the *X*4 map.

Excluding the map based on the limited-basis-set *T*3 calculation, three theoretical maps are available for comparison, the *T*2 dynamic map and the *T*1 and *T*2 static distributions (Fig. 3). Though the *T*1 and *T*2 static maps are at different contour intervals, peak shapes can be seen to agree well as did the peak heights discussed earlier. The thermally smeared *T*2 map at 0·05 e Å^{-3} contour (Fig. 3*c*) shows peak shapes which strongly resemble the *X*3 experiment, especially in the C–C bond.

A most interesting feature is observed in all experiments in the lone-pair region of the water-molecule oxygen atom, the lone-pair peak being clearly polarized into the short hydrogen bond, rather than being symmetric with respect to the plane of the isolated water molecule. The result of the *X*2 experiment in

a plane perpendicular to the water molecule bisecting the HOH angle is shown in Fig. 4.

In summary, though overall features agree well, differences in detail exist which caution against over-interpretation of detail observed in experimental electron density maps.

Conclusions

The following are the main conclusions drawn from this study.

(1) Large differences between the vibrational tensor elements U_{ii} can often not be corrected by a scaling of all temperature parameters of a set. The differences are such that they will affect translational amplitudes more strongly than librational amplitudes when a rigid-body analysis is performed.

(2) High-order temperature parameters from X-ray data above $\sin\theta/\lambda = 1$ Å^{-1} are 2–4% lower than parameters obtained from all data. Since there are no anisotropic differences between the two sets $X-X$ maps may be less biased by systematic errors in the temperature parameters than $X-N$ maps except, of course, in regions near hydrogen atoms, where neutron data remain essential.

(3) Positional parameters are reproducible in this study to precisions of 0·001 Å or better. Average discrepancies between some of the experiments are only 0·0005 Å.

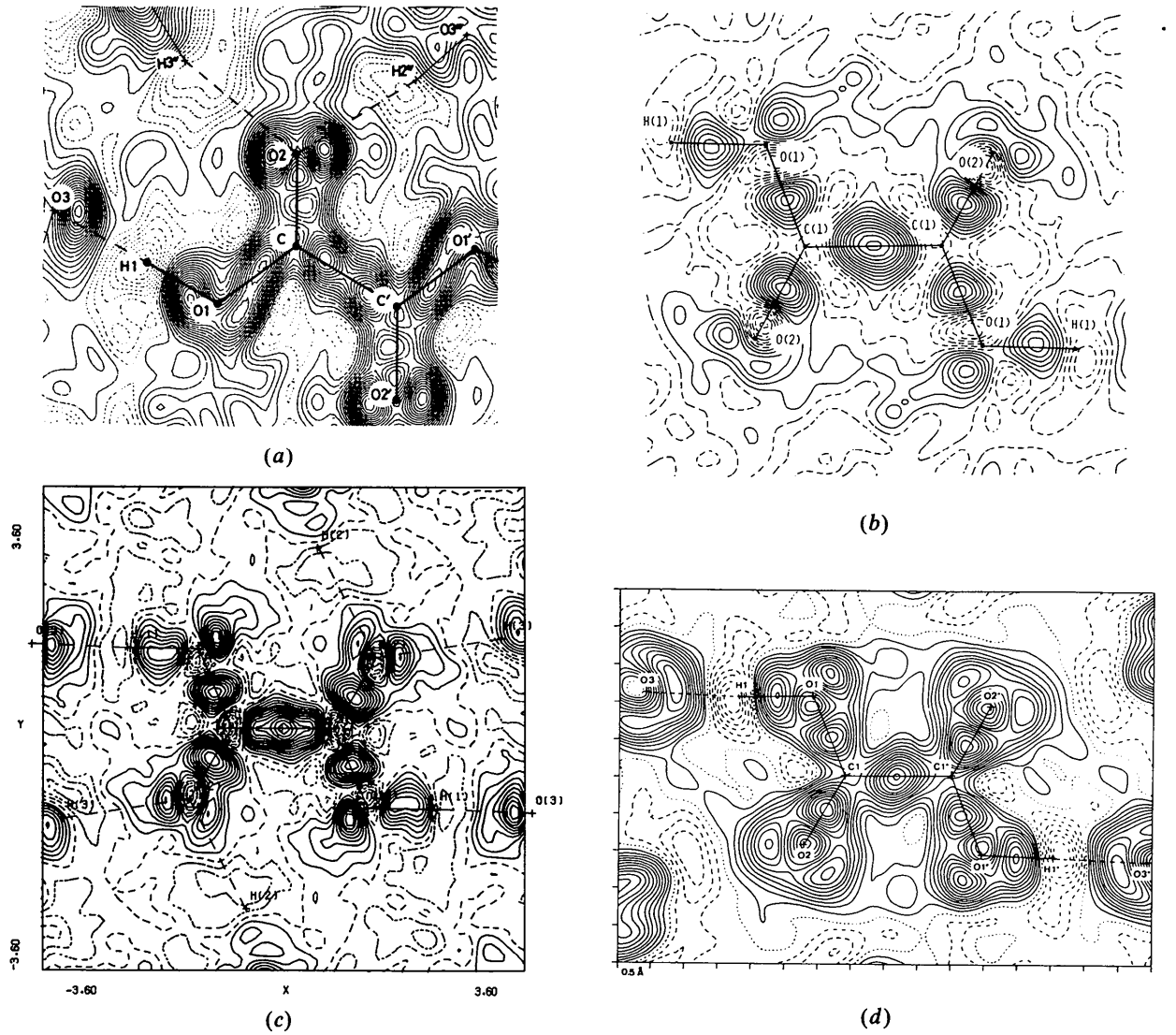

Fig. 2. Experimental deformation density maps in the plane of the oxalic acid molecule. All contours at 0·05 e Å^{-3}. (*a*) *X*1, negative contours dashed. Data with $\sin\theta/\lambda < 0{\cdot}85$ Å^{-1} included. (*b*) *X*2, zero and negative contours dashed. Data with $\sin\theta/\lambda < 1{\cdot}05$ Å^{-1} included. (*c*) *X*3, zero and negative contours dashed. All data included ($\sin\theta/\lambda < 1{\cdot}20$ Å^{-1}). (*d*) *X*4, negative contours dashed, zero contours dotted. Data with $\sin\theta/\lambda < 0{\cdot}7$ Å^{-1} included.

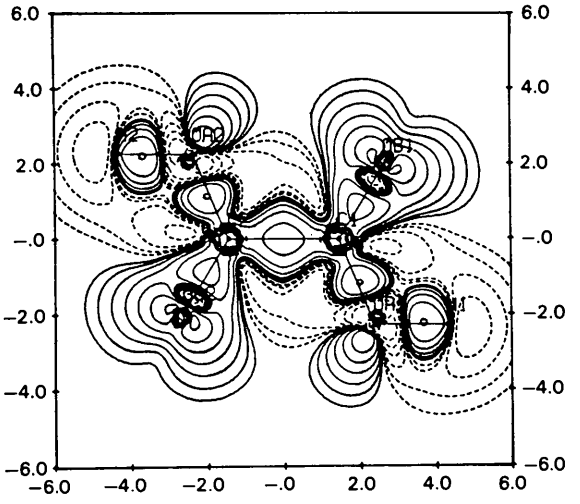

(*a*)

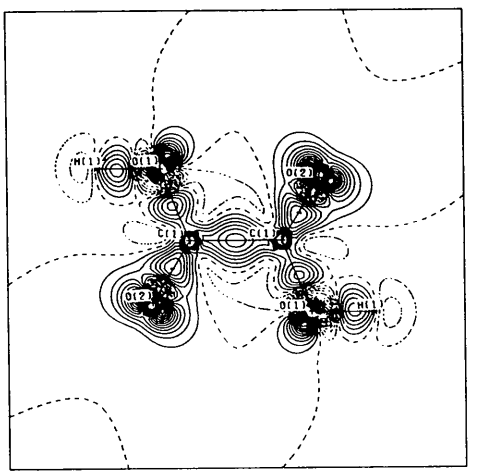

(*b*)

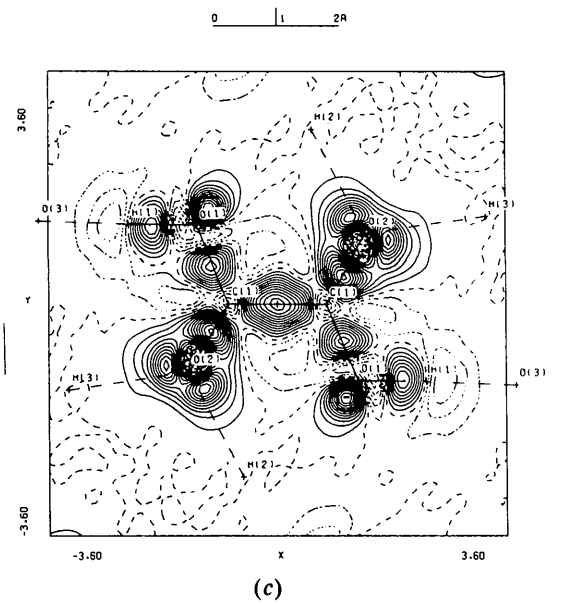

(*c*)

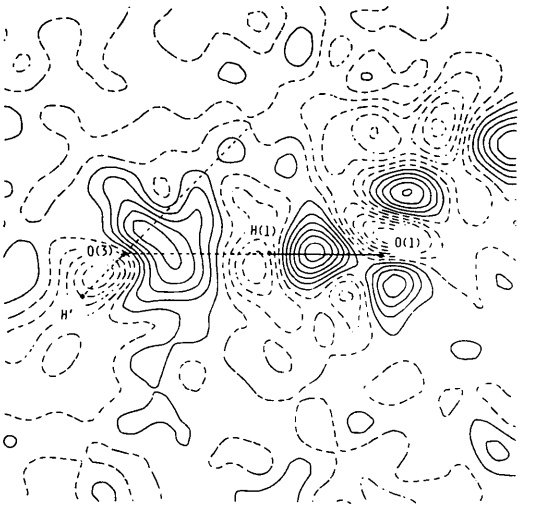

Fig. 4. *X*2 dynamic density in a plane perpendicular to the water molecule bisecting the HOH angle. Contours as in Fig. 2(*b*). The horizontal dotted line represents the projection of the hydrogen bond. The inclined line is the line of intersection with the water-molecule plane.

(4) Chemically significant features in the electron density maps are observed in all studies and are qualitatively reproducible. Peak heights between the best of the experiments surveyed here appear reproducible to within about 0·15 e Å^{-3}, though peak shapes and locations of the maxima differ in detail. Details of the experimental distribution should be interpreted with great caution.

(5) The biggest discrepancies between theory and experiment occur in the lone-pair-peak regions where peaks are higher in the theoretical maps. The quantitative comparison is hampered, however, by potential inadequacies in the thermal-motion treatment.

Note added in proof: One of the experiments included in this survey has been described recently in a separate article (Dam, Harkema & Feil, 1983). This article also reports the effect of a TDS correction on the density maps.

Support from the US National Science Foundation is gratefully acknowledged. Research at Brookhaven National Laboratory was performed under contract with the US Department of Energy. One of the studies was supported by the Netherlands Foundation for Chemical Research (SON) with financial aid from the Dutch Organization from the Advancement of Pure Research (ZWO). We would also like to thank Dr A. Kvick for his critical reading of the manuscript.

Fig. 3. Theoretical deformation density maps in the plane of the oxalic acid molecule. (*a*) *T*1 static density. First contours at ±0·0025 e a_0^{-3} (~0·0169 e Å^{-3}), neighboring contours differ by a factor 3. (*b*) *T*2 static density. Contours at 0·10 e Å^{-3} with zero and negative contours dashed. (*c*) *T*2 dynamic density. Contours at 0·05 e Å^{-3} with zero and negative contours dashed.

References

ALLIBON, J. R., FILHOL, A., LEHMANN, M. S., MASON, S. A. & SIMMS, P. (1981). *J. Appl. Cryst.* **14**, 326–328.

BACON, G. E. (1975). *Neutron Diffraction.* Oxford: Clarendon Press.

BECKER, P. J. & COPPENS, P. (1974). *Acta Cryst.* A**30**, 129–147.

BECKER, P. J. & COPPENS, P. (1975). *Acta Cryst.* A**31**, 417–425.

COPPENS, P. (1975). *International Review of Science, Ser.* 2, Vol. 11, pp. 21–56. London, Boston: Butterworth.

COPPENS, P. (1982). In *Electron Distributions and the Chemical Bond*, edited by P. COPPENS & M. B. HALL, pp. 61–94. New York: Plenum.

COPPENS, P. & SABINE, T. M. (1969). *Acta Cryst.* B**25**, 2445–2451.

COPPENS, P., SABINE, T. M., DELAPLANE, R. G. & IBERS, J. A. (1969). *Acta Cryst.* B**25**, 2451–2458.

CROMER, D. T. & LIBERMANN, D. (1970). *J. Chem. Phys.* **53**, 1891–1898.

CROMER, D. T. & WABER, J. T. (1965). *Acta Cryst.* **18**, 104–109.

DAM, J., HARKEMA, S. & FEIL, D. (1982). Private Communication.

DAM, J., HARKEMA, S. & FEIL, D. (1983). *Acta Cryst.* B**39**, 760–768.

DELAPLANE, R. G. & IBERS, J. A. (1969). *Acta Cryst.* B**25**, 2423–2437.

DITCHFIELD, R., HEHRE, W. J. & POPLE, J. A. (1971). *J. Chem. Phys.* **54**, 724–728.

FRAZER, B. C. & PEPINSKY, R. (1953). *Acta Cryst.* **6**, 273–285.

HAMILTON, W. C. (1964). *Statistics in Physical Science.* New York: Ronald Press.

HARKEMA, S., DAM, J., VAN HUMMEL, G. J. & REUVERS, A. J. (1980). *Acta Cryst.* A**36**, 433–435.

HUTCHINGS, M. T., SCHULHOF, M. P. & GUGGENHEIM, H. J. (1972). *Phys. Rev. B*, **5**, 154–158.

International Tables for X-ray Crystallography (1974). Vol. IV. Birmingham: Kynoch Press.

JOHNSON, C. K. (1965). *ORTEP.* Report ORNL-5138. Oak Ridge National Laboratory, Tennessee.

KOESTER, L. (1977). In *Springer Tracts in Modern Physics*, Vol. 80, edited by G. HÖHLER, p. 36. Berlin, Heidelberg, New York: Springer.

LEHMANN, M. S. & LARSEN, F. K. (1974). *Acta Cryst.* A**30**, 580–584.

POPLE, J. A. & BINKLEY, J. S. (1975). *Mol. Phys.* **29**, 599–611.

ROOTHAAN, C. C. J. (1951). *Rev. Mod. Phys.* **23**, 69–89.

SABINE, T. M., COX, G. W. & CRAVEN, B. M. (1969). *Acta Cryst.* B**25**, 2437–2441.

STEWART, R. F., DAVIDSON, E. R. & SIMPSON, W. T. (1965). *J. Chem. Phys.* **42**, 3175–3187.

THORNLEY, F. R. & NELMES, R. J. (1974). *Acta Cryst.* A**30**, 748–757.

Acta Cryst. (1984). A**40**, 195–200

A New Approach to Structure Determination of Large Molecules by Multi-dimensional Search Methods

BY DOV RABINOVICH AND ZIPPORA SHAKKED

Department of Structural Chemistry, The Weizmann Institute of Science, Rehovot 76100, *Israel*

(*Received* 10 *January* 1983; *accepted* 1 *September* 1983)

Abstract

A new multi-dimensional search approach, incorporating packing criteria with *R*-factor calculations for low-resolution X-ray data, proved to be extremely efficient for the solution of large molecular structures. A computer program, *ULTIMA*, based on this approach solved *ab initio* the structure of a double-helical DNA octamer and also reproduced the correct solutions of a double-helical DNA dodecamer and of a tRNA molecule (322, 486 and 1652 non-hydrogen atoms, respectively). The efficiency of the procedure is enhanced by using group scatterers in lieu of individual atoms. The method allows, for more complex structures, the separation of parameters in the multi-dimensional space, either by using one-dimensional reflection data or by approximating the entire molecule to a 'super-atom' scatterer.

Introduction

We have shown (Rabinovich & Schmidt, 1966) that small molecular structures can directly and efficiently be solved by a systematic search procedure (*SEARCH*) using geometrical criteria such as global molecular packing considerations and hard-sphere atom–atom contacts. The method owes its efficiency to a set of multi-level sieving operations, by means of which only a limited number of accepted trial structures are left for further examination by structure-factor calculations.

This procedure proved, however, to be inefficient for large molecular structures since it was time consuming as a result of the large number of atoms. It also yielded too many accepted trial structures because of the rather small number of intermolecular atom–atom contacts resulting from the fact that a large fraction of the unit-cell volume consists of solvent molecules. We have, therefore, developed a new multi-dimensional search approach, incorporating global packing criteria with structure-factor calculations for very-low-resolution X-ray data, which proved to be extremely efficient for the solution of large molecules. A computer program, *ULTIMA*, based on this approach, solved *ab initio* the structure

0108-7673/84/030195-06$01.50